Initial response of a turbulent channel flow to spanwise oscillation of the walls

Maurizio Quadrio[1] and Pierre Ricco[2]

Dipartimento di Ingegneria Aerospaziale del Politecnico di Milano,
via La Masa 34-20158 Milano, Italy
E-mail: maurizio.quadrio@polimi.it

Abstract. The transient behaviour of a turbulent channel flow suddenly subjected to spanwise harmonic oscillations of the walls is numerically studied by means of direct numerical simulations of the incompressible Navier–Stokes equations. It is well known that this movement of the walls produces a sustained and significant reduction in turbulent friction; in this paper we focus on the early stages of the motion after the start of the oscillations when the fully developed state has not yet established.

It is found that at the very beginning of the oscillatory motion the streamwise wall shear-stress remains constant for a short time interval, the length of which depends on the parameters defining the oscillation. A spanwise velocity profile starts to develop, almost coincident with the analytical laminar solution for the sudden start-up of harmonic oscillations of the wall.

The spanwise flow fully adapts to the new forcing after about one oscillation period, whilst the longitudinal flow is still evolving towards its long-term drag-reducing condition. The duration of the transient for the longitudinal wall shear-stress is significantly longer, and is found to be independent from the oscillation period, at least for the range of periods considered, but to be notably related to the maximum wall velocity. The implications of this last new finding are noteworthy, since it appears that some of the available experimental data concerning drag reduction measurements over an oscillating wall might be biased by transient effects, especially for the highest values of wall velocity.

Moreover, we observe that the turbulent wall friction and the turbulence statistics change from their initial condition to their long-term behaviour following a non-monotonic path. The paper concludes with two- and three-dimensional flow visualizations of the turbulent flow fields immediately after the start of the oscillations. The use of a moving reference frame, in motion with a speed that is comparable to the convection velocity of the turbulent

---

[1] Author to whom any correspondence should be addressed.
[2] Present address: Department of Mathematics, Imperial College, 180 Queen's Gate, London SW7 2BZ, UK.

structures in the near-wall region, allows a clear appreciation of the dynamics of the turbulent flow, thanks to the removal of the purely convective motion. The laminar spanwise flow is removed from the computed turbulent flow fields, in order to clarify the dynamics of the near-wall turbulent structures. The initial interaction of turbulence with the moving wall is then vividly described.

PACS numbers: 47.27.Eq, 47.27.Nz, 47.27.Rc

Contents

1. Introduction

In turbulent boundary layers, channel and pipe flows, a persistent skin-friction reduction can be achieved by means of spanwise wall oscillations, as first shown by Jung *et al* [1]. These modified turbulent flows are of great theoretical and practical interest: they arise in several applied problems, namely in flows around oscillating bodies, in boundary layers with fluctuating free-stream currents and in three-dimensional boundary layers, and a net drag reduction can be achieved, as shown by Baron and Quadrio [2] and Quadrio and Sibilla [3]. Recently, many researchers have studied these wall-bounded turbulent flow problems, both through direct numerical simulations (DNSs) ([1, 3] and references therein) and experimentally ([4]–[6] and references therein), focusing their attention on the flow regime which takes place well after the start-up of the oscillations, when the flow has fully adapted to the new condition and shows a statistically steady-state character, with stationary time-averaged quantities.

In this paper we devote our attention to the initial, transient period which immediately follows the start-up of the oscillations. This evolving flow is of considerable interest *per se*, since the interaction between the moving wall and the turbulence flow, which is known to significantly alter the turbulence regeneration cycle near the wall, can be better appreciated in the early stages of the surface motion, when the turbulent flow starts changing to the new quasi-equilibrium state from its original state. The analysis of the initial evolution of the flow should then allow for a more detailed evaluation of the mechanisms of the interaction between the solid wall and turbulence currently proposed in the literature. More generally, the development of a turbulent flow starting from a given initial equilibrium condition and evolving towards a *different* final equilibrium state still lacks a thorough description. We can mention the paper by He and Jackson [7], who experimentally studied the complex evolution of turbulence in pipes subjected to

a ramp-like change in the flow rate. Kannepalli and Piomelli [8] examined the three-dimensional turbulent boundary layer that develops over a flat plate when a section of the plate moves at a constant speed in the transversal direction, and studied both the adaptation of the flow to a three-dimensional configuration and its recovery towards two-dimensional behaviour. Jiménez *et al* [9] observed the evolution of the friction coefficient in a turbulent channel flow where one of the walls is suddenly made permeable, considering both the initial transient and the final, faster transient when the porosity is switched off. Chung and Luo [10] recently examined the effect of a sudden decrease in the pressure gradient of a turbulent channel flow on turbulence statistics.

In addition to these few, recent research papers, other, available investigations deal with either the study of suddenly perturbed turbulent flows that eventually relax back to the initial state, or the analysis of long-term modifications of natural turbulent flows that disregard the initial transient regime. For example, the papers by Moin *et al* [11], Sendstad and Moin [12], Coleman *et al* [13] and Le *et al* [14] belong to the first case, and concern the sudden application of a spanwise pressure gradient or a spanwise shear to a turbulent wall flow which realigns itself to the new mean flow direction after a temporary three-dimensional regime. On the other hand, the papers by Orlandi and Fatica [15] concerning the turbulent pipe flow in steady rotation around the longitudinal axis, and by Spalart [16] presenting the three-dimensional turbulent boundary layer over an indefinite plane wall generated by an external velocity with a constant modulus and a wall-parallel direction changing with constant angular velocity, are examples of the latter case. The final state is indeed three-dimensional and different from the initial one, but the initial start-up of the rotating motion is not considered. Most of the previous papers on turbulent flows with wall oscillations belong to this second category, and do not consider the start-up of the oscillatory motion.

Very limited information regarding the initial transient of a turbulent channel flow modified by spanwise wall oscillations can be found in the numerical study by Jung *et al* [1], who reported the behaviour of streamwise wall shear-stress as a function of time from the beginning of the wall movement, but did not deal with the very first instants of motion. More recently, Dhanak and Si [17] briefly discussed the start-up transient for the streamwise skin-friction, in a paper based on the numerical solution of a simplified version of the full Navier–Stokes equations. Experimentally, the related analysis of the spatial transient has received even less attention. Only Choi *et al* [18] measured the variation of the local skin-friction coefficient with the distance from the leading edge of the oscillating surface, but only for a single set of oscillatory parameters. The measured streamwise distribution of the skin-friction coefficient along the moving section of the wall was scattered, and it was not clear whether the flow had fully developed to the new equilibrium state at any downstream position. The temporal transient has never been considered in a laboratory setting, with the exception of the note by Choi in [5], where the temporal transient is said to be one-oscillation-cycle long, regardless of the oscillation period and the maximum wall velocity.

In this paper we investigate, through the DNS of the incompressible Navier–Stokes equations in the geometry of the indefinite plane channel, the evolution of the turbulent flow from the initial unperturbed state to the final drag-reducing condition induced by the oscillation of the walls. The paper is organized as follows. A description of the numerical method and of the computational procedures is presented in section 2. The effects of the oscillation on the two components of the turbulent wall shear-stress at the very beginning of the wall motion are illustrated in section 3, whereas the process through which the flow reaches its new, fully established regime is described in section 4 in terms of longitudinal and spanwise wall shear-stress and turbulence statistics. Section 5 presents two- and three-dimensional flow visualizations, which allow a clear visual understanding of the interaction between the moving wall and wall turbulence; this interaction clearly emerges thanks to the wall motion being imposed on an initially unperturbed flow. Lastly, section 6 is devoted to our conclusions.
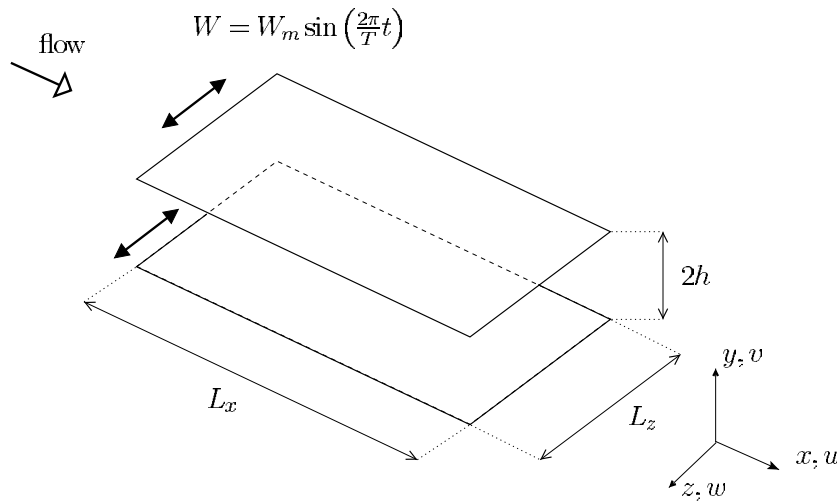
Figure 1. Schematic of the physical domain and the coordinate system.

2. Numerical method and computational procedures

Only the essential features of the numerical method and of the computing system will be outlined here, and the interested reader should refer to Quadrio and Luchini [19] for further details.

The computer code is a pseudo-spectral DNS code based on a mixed discretization: Fourier expansions for the homogeneous (streamwise and spanwise) directions and fourth-order accurate, compact finite differences schemes over a variable-spacing mesh for the wall-normal coordinate. Figure 1 presents a sketch of the computational domain and the coordinate system used. The numerical method is based on the formulation of the incompressible Navier–Stokes equations, presented for example by Kim *et al* [20], in terms of two, scalar independent equations for the wall-normal components of the velocity and vorticity vectors, with the pressure removed from the equations.

The computer code has been designed with computational efficiency in mind. The most accurate similar codes described in the literature are essentially based on the architectural design described in the pioneering paper by Kim *et al* [20], requiring at least 40% more memory for a given problem size. The present code is able to take advantage of both shared-memory SMP architectures and a number of distributed-memory machines, and can subdivide memory requirements between these computing units. On top of the code, a dedicated computing system constructed by SMP Personal Computers has been designed and built at the Dipartimento di Ingegneria Aerospaziale del Politecnico di Milano; each node of the system is equipped with two Intel Pentium III CPU at 733 MHz and 256 MB RAM, and eight such machines are linked in a connection topology which avoids any hub or switch. Fast Ethernet cards allow the calculations not to be communication bound.

For the present study, the no-slip boundary condition for the spanwise velocity component at the two walls has been modified in the following form:

$$W = W_m \sin\left(\frac{2\pi}{T}t\right) \tag{1}$$

where the spanwise velocity, W, of the wall is a sinusoidal function of time t with the prescribed period T and amplitude W_m.

The Reynolds number used in the present work is defined as $Re_\tau = u_\tau h/\nu$, where u_τ is the friction velocity of the unperturbed case, h is half of the channel height and ν is the kinematic viscosity of the fluid. The simulations are performed for a value of the Reynolds number of

$Re_\tau = 200$. The flow rate in the streamwise direction is kept constant, thus allowing the space-averaged streamwise friction to fluctuate in time, and a null value for the spanwise mean pressure gradient is imposed.

The streamwise length of the computational domain is discretized with 160 Fourier modes, and 128 of them are used for the spanwise direction; the number of collocation points in the wall-normal direction is 129. Following [21], the dimensions of the computational domain are $L_x = 4\pi h$ and $L_z = 4/3\pi h$; the spatial resolution is $\Delta x^+ = 15.7$, $\Delta z^+ = 6.5$ and $\Delta y^+ = 0.8$–5.4 (unless otherwise stated, the $+$ superscript indicates quantities that are made dimensionless with inner variables, i.e. with the friction velocity of the unperturbed case and the kinematic viscosity of the fluid). The resolution in wall units becomes much higher when drag reduction takes place, due to the significant drop in the friction velocity: for example with $W_m^+ = 18$ and $T^+ = 125$ the resolution in wall units when the flow reaches the minimum level of drag is $\Delta x^+ = 9.4$, $\Delta z^+ = 3.9$ and $\Delta y^+ = 0.5$–3.2 if the actual u_τ is used.

Time integration of the equations is performed with the classic partially implicit approach, using a third-order, low-storage Runge–Kutta method for the convective terms and a second-order, implicit Crank–Nicolson scheme for the viscous terms. The time step size is $\Delta t^+ \approx 0.15$.

In order to check the sensitivity of the numerical results to the spatial discretization, we performed a resolution study for the case with oscillatory conditions given by $W_m^+ = 18$ and $T^+ = 125$, employing 256 Fourier modes in the streamwise direction, 161 in the spanwise direction and 257 collocation points in the wall-normal direction, i.e. four times the number of degrees of freedom of the other calculations. This check definitely demonstrated that the transient behaviour of the flow is essentially insensitive to the increase in spatial resolution. The long-term time histories of the flow variables are different, due to the intrinsic nature of the Navier–Stokes equations, but the time-averaged value of the streamwise friction is, in practice, stationary, i.e. with a difference well below 1% when computed over a time interval of more than 5000 viscous time units.

3. Early transient

In this section we describe the initial instants after the beginning of the wall motion. The typical timescale is $t^+ = \mathcal{O}(10)$, i.e. much shorter than the time needed by the flow to adapt to its new conditions, which is $t^+ = \mathcal{O}(1000)$. Longer timescales will be considered in the next section.

3.1. Longitudinal friction

The time histories of the space-averaged longitudinal shear stress $\tau_x^+ = \partial u^+/\partial y^+$ from the start of the wall motion until $t^+ = 30$ are depicted in figures 2 and 3. Data over the two walls have been ensemble averaged for a better statistical sample.

In the case of figure 2 the wall moves with $W_m^+ = 18$, and the oscillation period is varied. It is evident that τ_x^+ is unaffected by the lateral motion of the wall until a characteristic diffusion time is reached, which apparently increases with the oscillation period with a $\sqrt{T}$ law. Then, the friction starts feeling the effect of the moving wall, and decreases at a rate which eventually becomes constant in time and independent of T.

Figure 3 shows the friction time history when the oscillation period is kept constant at $T^+ = 125$, and the maximum wall velocity is varied. The time needed for the effect of the oscillation to be felt now varies with the inverse of $\sqrt{W_m}$. Similarly to the cases reported in figure 2, at later times the friction decrease rate becomes constant. When the maximum wall velocity is varied we note, however, the significant difference that the constant decrease rate strongly depends on W_m, being higher at higher W_m.
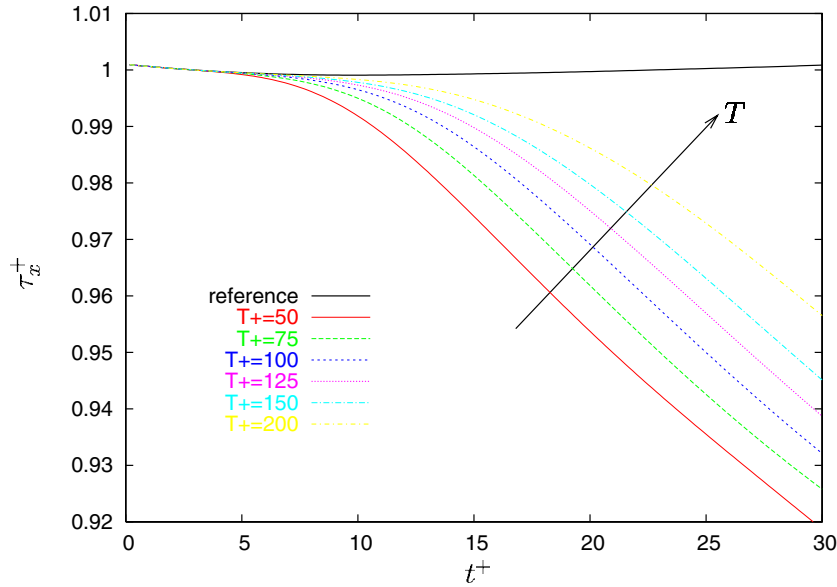
Figure 2. The early time history (ensemble averaged over the two walls) of the longitudinal wall shear-stress τ_x^+ compared to the stationary case (black curve), during the beginning of the oscillation, at different periods. The maximum wall velocity is $W_m^+ = 18$.

From both figures 2 and 3 it is evident how the drag-reducing effect of the oscillation is not felt during the very first instants. This is because the vertical distance to which the wall motion extends its influence is still smaller than the average height of the low-speed streaks, i.e. near-wall structures elongated in the streamwise direction, existing approximately at a distance from the solid wall between $y^+ = 3$ and 10. Spanwise shear stresses generated at the wall take some time to diffuse to the interior and to significantly drag laterally the low-speed streaks, so disrupting their spatial coherence with the overriding quasi-streamwise vortical structures, which typically exist at $y^+ > 20$, as shown for example by Jeong *et al* [22]. This is consistent with the suggestion, put forward by Quadrio and Sibilla [3], that the relative lateral displacement of low-speed near-wall regions and quasi-streamwise vortices is related to the reduction in friction drag.

In the recent literature a similar time history of wall shear-stress has been reported by Dhanak and Si [17], as a function of only the oscillation period. Similarly to the present results, they found an initial time interval where the stress remains constant. However, their study was based on a very simplified version of the Navier–Stokes equations, in which the longitudinal variations of the flow are neglected; probably because of the considerable simplifications embodied in their equations, in [17] the duration of this initial phase of constant shear did not appear to depend at all on the oscillation period, and was underestimated at least by a factor of two.

3.2. Spanwise friction

After the wall has been set in motion, a spanwise boundary layer develops, which can be observed from the numerical simulations. Here we show that this spanwise flow, and in particular the spanwise component of the wall friction, coincides with the analytical solution of the laminar boundary layer equations under the same condition of wall set in sinusoidal motion from rest.
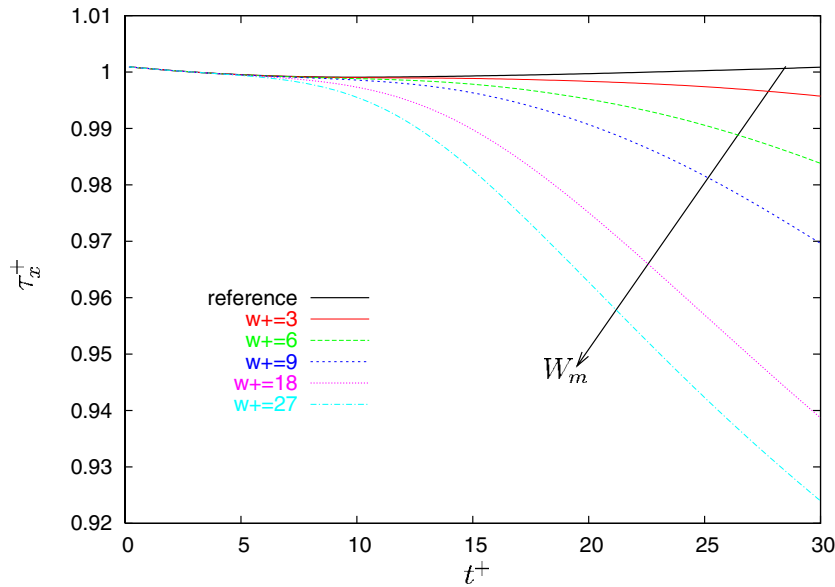
Figure 3. The early time history (ensemble average over the two walls) of longitudinal wall shear-stress τ_x^+ compared to the stationary case (black curve), during the beginning of the oscillation, at different maximum wall velocities. The period is $T^+ = 125$.

Similar results have been reported by Quadrio and Sibilla [3] for oscillating pipe flows, and by Choi and Clayton in [23] for a planar free-stream boundary layer over an oscillating wall, but limited to the quasi-stationary turbulent regime which takes place after the initial transient disappears. A similar qualitative idea, in the more general context of three-dimensional boundary layers, can be found in [14]. In terms of spatial evolution, in [8] a transversal boundary layer decoupled from the streamwise evolution of the flow and characterized by a thickness increasing with $x^{1/2}$ has been reported for the turbulent flow over a flat plate with a section in uniform spanwise motion.

Here we are able to develop a quantitative analysis. Let us first rescale the time and wall-normal coordinates as

$$\tau = \frac{2\pi}{T}t; \qquad \eta = \frac{y}{\sqrt{\nu T/(2\pi)}}$$

so that the wall movement is described by $W(\tau) = W_m \sin\tau$. The well known steady-state solution of this flow, known as the Stokes second problem, expresses the laminar spanwise velocity profile as a function of the similarity variables η and τ as

$$\frac{w(\eta,\tau)}{W_m} = \mathrm{e}^{-\eta/\sqrt{2}} \sin\left(\tau - \frac{\eta}{\sqrt{2}}\right). \tag{2}$$

As reported, for example, in [24], when the wall starts moving from rest, the solution can be expressed as the steady-state term (2) corrected by an additional transient term, which must vanish as $\tau \to \infty$ (i.e. when $t \to \infty$)

$$\frac{w(\eta,\tau)}{W_m} = \mathrm{e}^{-\eta/\sqrt{2}} \sin\left(\tau - \frac{\eta}{\sqrt{2}}\right) + \frac{1}{\sqrt{4\pi\tau}} \int_0^\infty f(y')(\mathrm{e}^{-(\eta-y')^2/4\tau} - \mathrm{e}^{-(\eta+y')^2/4\tau})\,\mathrm{d}y'. \tag{3}$$

In equation (3), the function $f(y')$ equals the value of the integral at $\tau = 0$, and is consequently given by

$$f(y') = e^{-y'/\sqrt{2}} \sin\left(\frac{y'}{\sqrt{2}}\right).$$

The above expression can be obtained by setting $\tau = 0$ in equation (2) and by noting that the transient part must be opposite to the steady-state solution at the beginning of the oscillation. The numerical integration of equation (3) shows that a spanwise boundary layer develops, whose thickness starts increasing proportionally to the square root of the kinematic viscosity of the fluid and of the time until $t^+ \approx 10$, and follows a linear trend at later times. This particular initial growth was expected, since it occurs in the analogous first Stokes problem, where the wall is impulsively set in motion at a constant velocity. It is also found that the viscous-diffusion distance depends neither on the oscillation period nor on the maximum wall velocity.

The increase with time of the quantity δ_{66}^+, defined as the distance from the wall where the velocity reaches 1/3 of the instantaneous wall velocity, is compared in figure 4 for the laminar solution (continuous curve) and the DNS results of the turbulent case (symbols). The oscillating conditions are $W_m^+ = 18$ and $T^+ = 125$. The turbulent results match very well the laminar ones, except for the slight discrepancy at very small t^+ caused by the spatially averaged spanwise velocity profile not being identically null in the turbulent case. As happened for the fully developed oscillating Stokes layer described by Quadrio and Sibilla [3] and by Choi et al [25] for turbulent pipe flows and by Choi and Clayton in [23] for a flat-plate boundary layer, the three-dimensional turbulent flow field does not alter the superimposed transverse flow, which follows closely the laminar solution.

At $t^+ = 5$ the spanwise velocity, which is $W^+ = 4.5$ at the wall, attains one third of this value at $y^+ = 2$. The fact that for the case under consideration $t^+ = 5$ is the time at which drag reduction begins to be felt (see figure 2) and that low-speed streaks populate the region $3 < y^+ < 10$ of the turbulent layer is a further indication that until $t^+ = 5$ these structures are not sufficiently immersed in the spanwise boundary layer to be laterally shifted, suggesting again that the effectiveness of wall oscillation for drag reduction purposes lies in the relative displacement between the streaks and the overriding quasi-streamwise vortices.

Figure 5 clearly illustrates how the transient laminar solution essentially coincides with the spatially averaged spanwise flow in the turbulent case. It is remarkable how the laminar profile maintains itself, notwithstanding the presence of significant fluctuations of the spanwise velocity component (see section 4.3 for a time-dependent visualization of the fluctuations of this component).

4. Long-term transient

The preceding section discussed the evolution of the flow over a timescale related to the short-time response of the flow to the modified condition at the boundaries. In the following we analyse the evolution of the flow over a longer timescale, sufficient for the wall turbulence to reach a new quasi-steady equilibrium condition.

4.1. Longitudinal friction

Figures 6 and 7 illustrate the temporal behaviour of the streamwise friction, for the same conditions of wall motion as those considered in figures 2 and 3, and ensemble averaged over the two walls.

In figure 6, where the oscillation period is varied and the maximum wall velocity is fixed, the decrease in drag only presents a slight dependence on T for $t^+ < 300$; at later times the curves asymptotically adjust to different long-term drag reduction values. While the oscillation
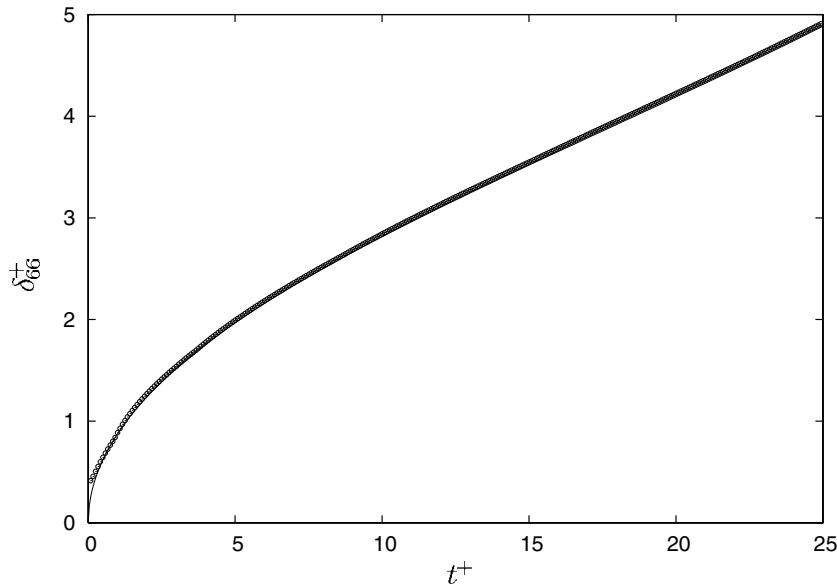
Figure 4. Spanwise boundary layer thickness δ_{66}^+ as a function of time during the start of the oscillations: comparison between the laminar analytical solution (continuous curve) and the turbulent DNS data (symbols). The oscillating conditions are $W_m^+ = 18$ and $T^+ = 125$.

period has no remarkable effect on the time history for the streamwise friction, the maximum wall velocity strongly affects its transient behaviour. This is clearly illustrated in figure 7, where the oscillation period is kept constant and W_m is varied. The time needed by the flow to adapt to its modified state appears to become significantly longer for higher W_m. This strong increase of the transient time with the maximum wall velocity is an important property of this flow which has not been hitherto reported in the literature. Its spatial counterpart, i.e. the distance from the leading edge of the oscillating section of the wall needed by the local friction to decrease from the unperturbed level to the diminished level brought about by the oscillation, has also received little experimental attention: only the paper by Choi *et al* [18] reported measurements of the local friction versus the streamwise coordinate, but only a single wall velocity was considered (namely $W_m^+ \approx 7$), thus preventing one from identifying a dependence of the transient length on W_m.

The importance of the present result can be realized by noting that, if the transient distance after the beginning of the oscillating section of the wall increases with W_m, in a laboratory experiment aimed at the measurement of drag reduction with spanwise oscillations the downstream position of the measuring probe must be such that the flow has already reached its fully developed condition *for the highest considered W_m value.*

For an estimation of the spatial transient length, temporal data can be converted into spatial data through a typical convection velocity at the wall of $\approx 10u_\tau$ (see, for example, [26]). From figure 7, a transient time of $t^+ = 200$–400 can be estimated for $W_m^+ = 6$, and this translates to 2000–4000 viscous lengths, in line with the length of the spatial transient observed by Choi *et al* [18] at similar W_m^+ values. The increase of the transient length with W_m (at $W_m^+ = 18$ it is approximately 2–3 times longer than at $W_m^+ = 6$, i.e. 6000–12 000 viscous lengths) implies that some published drag reduction measurements, reported, for example, in [4, 5, 18, 27, 28], and particularly those at high values of W_m might have been conducted insufficiently downstream from the leading edge of the oscillating section of the plate to be free from transitional effects.
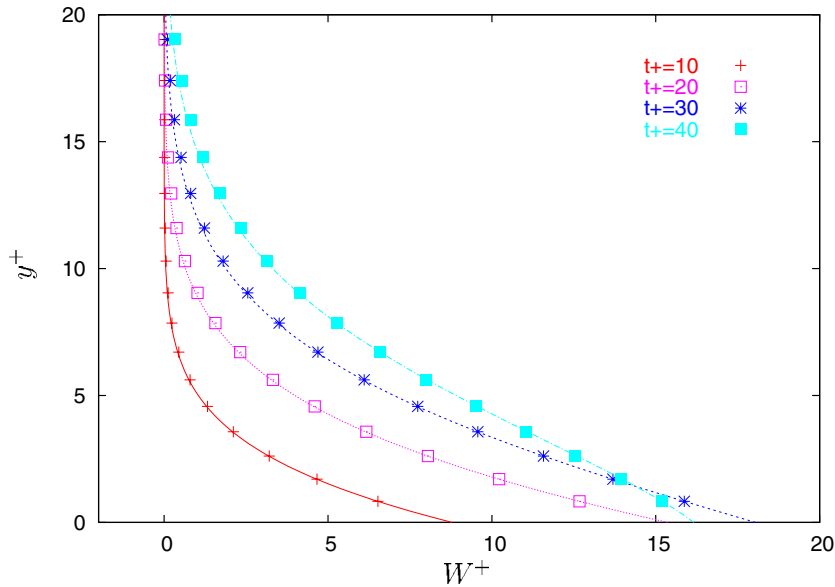
Figure 5. Spanwise velocity profiles at different time points during the start of the oscillations. Comparison between the analytical laminar solution (continuous curves) and DNS data (symbols). The oscillating conditions are $W_m^+ = 18$ and $T^+ = 125$.

Indeed, in none of the mentioned cases did the location of testing along the streamwise coordinate vary, whereas both W_m and T substantially did. The testing distances from the leading edge of the moving walls were reportedly 2650 viscous lengths in [18] and [5] (W_m^+ up to 13), 3500 in [4] and [27] (W_m^+ up to 16) and 4200 in [28] (W_m^+ up to 17).

4.2. Spanwise friction

The time history of the spanwise wall shear-stress $\tau_z^+ = \partial w^+ / \partial y^+$ is reported in figure 8, where the analytical laminar solution and the DNS data for one and a half oscillation periods are compared. Two oscillating conditions are considered: $W_m^+ = 18$ and $T^+ = 125$, and $W_m^+ = 4.5$ and $T^+ = 20$. The shear stresses are made non-dimensional by means of the maximum spanwise wall shear-stress $\tau_{z,m}^+$, obtained from the analytical solution of the second Stokes problem, i.e.

$$\tau_{z,m}^+ = W_m^+ \sqrt{\frac{2\pi}{T^+}} \tag{4}$$

and they are plotted versus the phase of the wall oscillation.

The comparison between the turbulent and laminar data is very good. The wall shear-stress anticipates in phase the wall velocity; for both the considered cases, the first peak of the shear stress is 15% lower than the maximum steady-state value, whereas the second peak is only 3% higher than the asymptotical value. The profiles rapidly adjust to the steady-state configuration. Slightly after the end of the first period of oscillation, the intensity of the negative peaks is about 1% lower in absolute terms than the corresponding asymptotical values. At this point, the shear stress profiles can be considered to have reached the steady-state character. Differently to the transient time, the maximum value of the spanwise wall shear stress depends both on W_m and T, as evident in equation (4).

We note that the transient time for τ_x^+ is related primarily to the maximum wall velocity (figure 7) and less significantly to the period of oscillation, whereas the transient time for τ_z^+
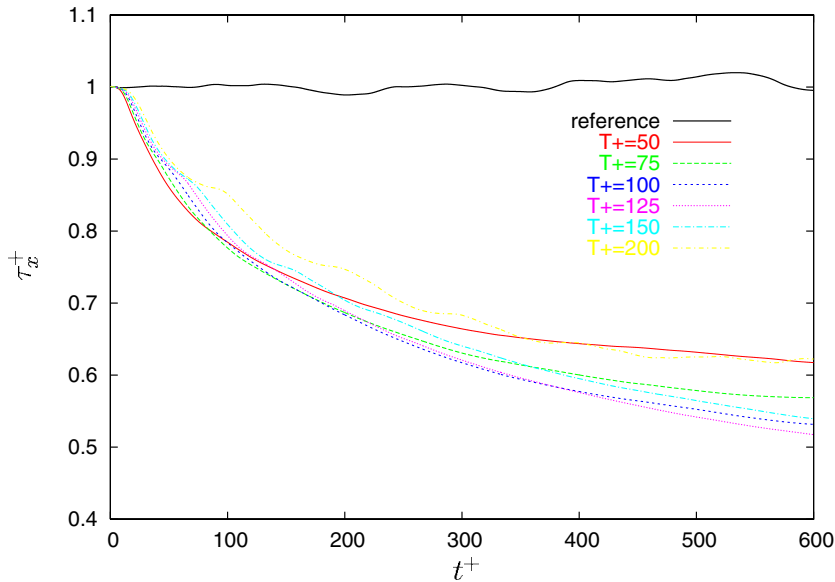
Figure 6. Late time history (ensemble averaged over the two walls) of the longitudinal wall shear-stress τ_x^+ compared to the stationary case (black curve), at different periods. The maximum wall velocity is $W_m^+ = 18$.
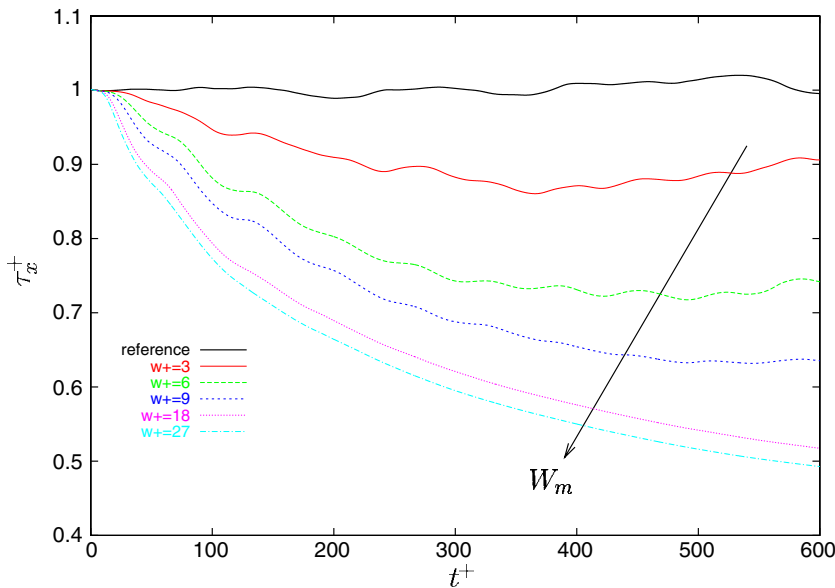

Figure 7. Late time history (ensemble averaged over the two walls) of the longitudinal wall shear-stress τ_x^+ compared to the stationary case (black curve), at different maximum wall velocities. The period is $T^+ = 125$.

is only influenced by the latter. For example, the transient time for the Stokes layer (one oscillation period) is much shorter than the four periods of oscillation, which are necessary for the streamwise shear stress to adjust to the new configuration when $W_m^+ = 6$ and $T^+ = 125$. This is because the regenerative cycle of near-wall turbulence adjusts to the forcing imposed by the wall motion in a much more complex (and slow) manner than the spanwise laminar layer.
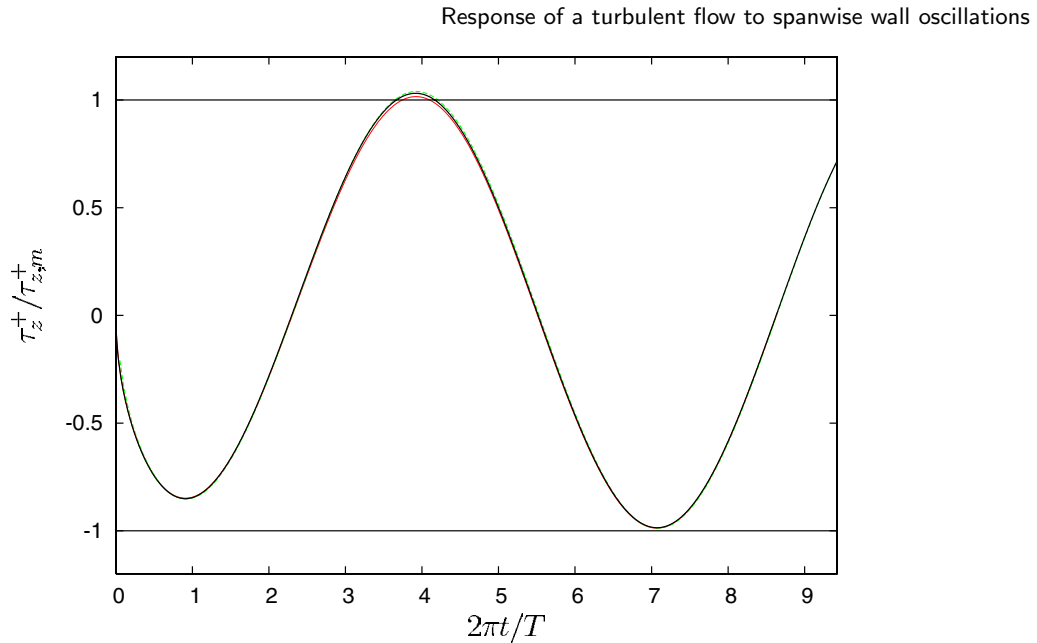
Figure 8. Spanwise wall shear-stress τ_z^+, normalized with the maximum oscillating stress $\tau_{z,m}^+$, as a function of the phase of the oscillation $2\pi t/T$: comparison between the analytical laminar solution (black curve), turbulent DNS data for $W_m^+ = 18$ and $T^+ = 125$ (red curve), and for $W_m^+ = 4.5$ and $T^+ = 20$ (green curve).

4.3. Turbulence statistics

Turbulence statistics are computed with a spatial average over the two homogeneous directions, and over the two halves of the channel for a further increased statistical sample. They are analysed in the following with the aim of better describing the initial effects of the oscillatory movement of the walls. The time-evolving profiles of various turbulence statistics are compared both to the reference profile without oscillations, and to the long-term, time-averaged results for oscillations given by $W_m^+ = 18$ and $T^+ = 125$. The latter are computed by averaging the statistics of 12 unrelated instantaneous flow fields (stored at a temporal separation of approximately 200 viscous time units) from a simulation started well after the end of the transient period. Most of the statistical quantities are non-dimensionalized by means of outer variables, namely with the bulk velocity U_b and the half-channel width h, whereas time and wall shear-stress are made non-dimensional by means of inner variables (but recall that the friction velocity is always the one of the reference case).

Figure 9 shows the temporal evolution of τ_x^+ during 4200 viscous time units after the beginning of the oscillations. There is a clear indication that this quantity presents a significant excursion below the long-term average, showing a local minimum of approximately 0.5 at $t^+ \approx 800$, before increasing again to the quasi-equilibrium average value of about 0.6 and fluctuating around it. In order to rule out a possible cause of this behaviour, namely the finite size of the computational box, we have performed two test cases doubling its length and width, while keeping the spatial resolution unchanged, i.e. also doubling the number of Fourier modes. For the case with a longer box of $L_x = 8\pi h$, we used 320 Fourier modes in the x direction, and 256 spanwise modes were employed for the simulation in a wider box with $L_z = 8/3\pi h$. All the test cases were conducted with the same Reynolds number and oscillatory conditions. The time histories of τ_x^+ for these cases are reported in figure 9, and fully confirm the previously
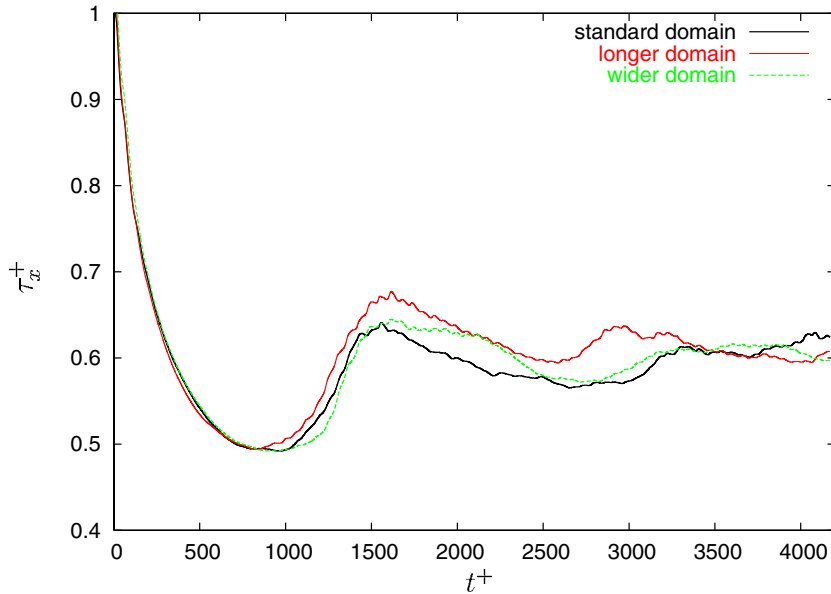
Figure 9. Long-term time behaviour (ensemble averaged over the two walls) of the longitudinal wall shear-stress for the standard simulation with $L_x = 4\pi h$ and $L_z = 4/3\pi h$ (black curve), for the longer domain with $L_x = 8\pi h$ (red curve) and for the wider domain with $L_z = 8/3\pi h$ (green curve). The oscillating conditions are $W_m^+ = 18$ and $T^+ = 125$.

described non-monotonic behaviour, thus excluding the effect of finite domain size. Thanks to the resolution check mentioned in section 2, we are also able to exclude any effects due to poor spatial resolution in the simulation.

Qualitatively related results have been reported by Le *et al* [14], and to some extent also by Kannepalli and Piomelli [8], where the spatial evolution of the friction is addressed. In [14] the temporal evolution of τ_x is described when the wall is impulsively set in constant spanwise motion: a small (10%) temporary decrease of τ_x is observed on a very short timescale of $t^+ \approx 50$, after which τ_x recovers to a higher quasi-equilibrium value. The present changes point to a different physical phenomenon. Indeed the initial effects of the three-dimensional skewing decay rather quickly, while the three-dimensional boundary layer reaches a quasi-equilibrium collateral situation. In contrast, the alternate oscillation of the wall (with a period of similar timescale) prevents the collateral situation being reached, and allows the turbulence producing cycle to be deeply affected. Eventually a quasi-equilibrium state is reached on a much longer timescale, and through a non-monotonic path.

This non-monotonic behaviour is not peculiar to only longitudinal friction, but it can be also observed for other turbulence statistics, as shown in figures 10–14. The local minimum of τ_x^+, however, occurs later in time than the local minima for the other statistics, thus indicating that the friction drag responds in a slower manner to the change of boundary conditions. This aspect is consistent with the findings of [14] over their shortest timescale.

Figure 10(a) shows the evolution of the profile of the root-mean-square value of the u velocity fluctuations versus the distance from the wall at different times (recall that the oscillation period is $T^+ = 125$). It can be seen how the inner regions are most rapidly affected by the wall motion, whereas the effects of the oscillation are felt throughout the whole channel only after two complete cycles. The maximum value of the distributions quickly relocates at higher vertical positions as
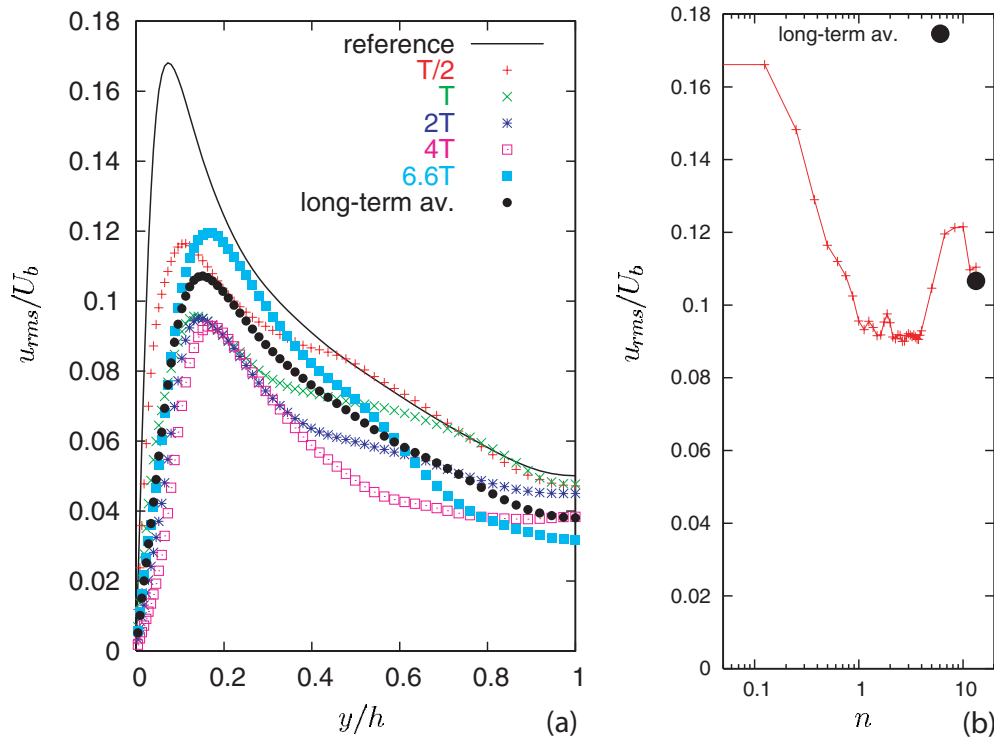
Figure 10. Evolution in time of the wall-normal distribution of u_{rms} (a), and peak value of the u_{rms} profiles versus the number, n, of oscillation cycles (b).

a consequence of the thickening of the viscous sublayer and of the buffer region produced by the wall oscillation.

The near-wall peak value of the profile is shown in figure 10(b) as a function of time, indicated here as the number of oscillation cycles; one can clearly see that the peak diminishes by as much as 60% of the unperturbed value after one period, and it remains at this level until approximately four cycles. It then increases slightly and eventually adjusts to the fully established level of 53% of the initial value. In [8] the evolution of the same profiles is described as a function not of time, but of the streamwise position over the moving section of the flat plate. Their results suggest a similar, non-monotonic decrease of the profile through successive oscillations and damping. Unfortunately the limited length of the moving section of the plate in [8] does not allow a more thorough comparison: their data appear to approach equilibrium after roughly 2000 viscous lengths after the leading edge of the moving section of the plate. If use is made again of a convection velocity of approximately $u^+ = 10$ [26], it appears that the transient can be followed for approximately 200 viscous time units, which amounts to $n = 1.6$ in figure 10(b).

The same quantities relative to the wall-normal velocity component (figure 11) present similar patterns, but with some quantitative difference when compared to the u component. The peak value of the profile is temporarily reduced at approximately 50% of the initial value after five periods, then increases slowly and adapts to the long-term state.

With respect to the spanwise velocity component (figure 12), a notable difference is that the peak value of w_{rms} presents an intense local maximum in correspondence of the first maximum wall displacement, namely immediately after the wall arrests its motion for the first time (see figure 13 for a more detailed view). This temporary peak is closer to the wall and 30% more intense than the initial value. The instantaneous increase of turbulent fluctuations in the spanwise direction is rapidly tamed by the turbulent flow: indeed, a smaller increment is detected
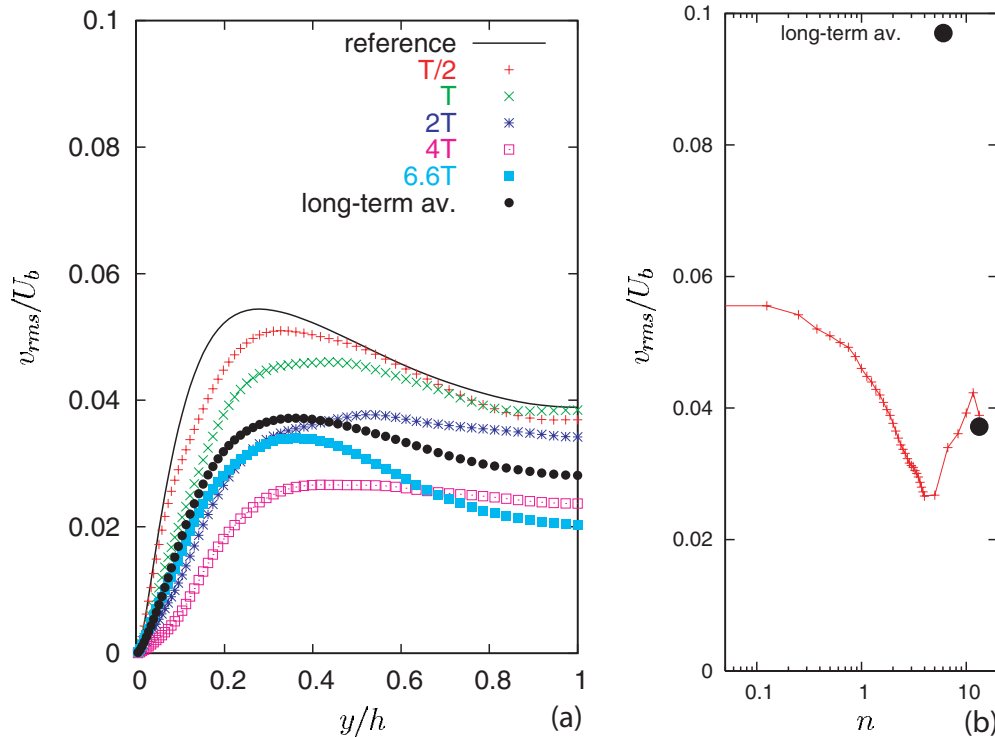
Figure 11. Evolution in time of the wall-normal distribution of v_{rms} (a), and peak value of the v_{rms} profiles versus the number n of the oscillation cycles (b).

when the velocity becomes null for the second time. A similar effect was observed by Sendstad and Moin [12], when a turbulent channel flow modified by an impulsively started transverse pressure gradient was studied through DNS, and was discussed by Quadrio and Sibilla [3] for the oscillating pipe flow. As will be better appreciated from the flow visualizations presented in section 5, this phenomenon is due to the transport, operated by quasi-streamwise vortices, of low-u, high-w fluid in the outward direction, and of high-u, low-w fluid towards the wall. Since the oscillations of the wall inhibit and modify the turbulence cycle, this phenomenon can be observed most clearly in the initial transient regime.

In figure 14 we report the same quantities for the Reynolds shear stress $-\overline{uv}$. This is the statistical quantity which shows the most significant change, diminishing as much as 70% of the unperturbed value, and then recovering to the long-term reduced value of 45%.

Further insight on the effects of the first stages of the wall oscillations can be gained by observing the most relevant production terms in the equation for the budget of the turbulent kinetic energy (TKE). The reduction of the TKE production term $P_{uu} = -2\,\overline{uv}\,\partial U/\partial y$ is shown in figure 15. Due to the decrease in the $\overline{uv}$ component of Reynolds stresses (already shown in figure 14), the peak value of P_{uu} reduces as much as 80% after four oscillatory cycles, whereas the long-term peak value shows a 65% reduction. Again, the behaviour of the profiles distinctly indicates that the adjustment to the different turbulent regime follows a non-monotonic path. It is also of interest to analyse the production term $P_{ww} = -2\,\overline{vw}\,\partial W/\partial y$ (see figure 16). This term is null when the wall is stationary, because of the absence of both the $\overline{vw}$ turbulent stresses and of the mean spanwise velocity profile; the same term vanishes again when the new fully developed state is fully established. As a response to the imposed oscillations, there occurs an intense production of vw fluctuations, which reaches its maximum after half of the first oscillation period.
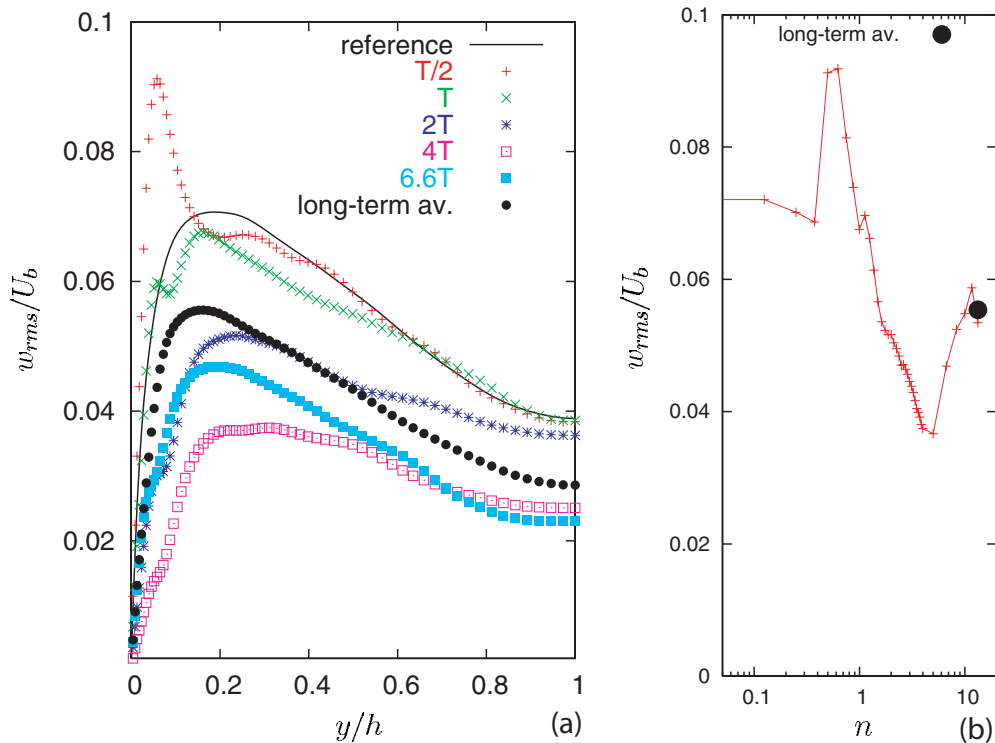
Figure 12. Evolution in time of the wall-normal distribution of w_{rms} (a), and peak value of the w_{rms} profiles versus the number, n, of the oscillation cycles (b).

The flow then slowly adjusts to the modifications induced by the wall motion, so that the $\overline{vw}$ correlation reduces again. This temporary change in turbulent production, primarily observed during the first oscillatory cycle, strongly influences the near-wall dynamics of w fluctuations. This significant effect has been previously reported in both figures 12 and 13, as the root-mean square of the w fluctuations presents a temporary peak soon after one quarter of the first cycle. More visual evidence is shown in figure 18.

5. Flow visualizations in the initial phase of the oscillations

Visualizations of flow fields computed from DNS offer a useful opportunity for understanding the modifications induced in the turbulent flow by the oscillations of the wall. In particular, the choice of examining the early stage of the motion allows for a better evaluation of the conceptual models that are proposed for explaining the drag reducing action of wall oscillations: the interaction of the wall movement is more evident since the initial flow field is unperturbed. Quadrio and Sibilla [3], on the basis of the analysis of long-term, phase-averaged turbulence statistics, have suggested that high-speed fluid convected transversally by the Stokes layer intrudes beneath low-speed regions, thus contributing to the homogenization of the u fluctuations. Quadrio and Sibilla's idea can be found also in [14], and it has been confirmed and expanded in the recent paper by Choi *et al* [25], where, based on conditionally averaged turbulence statistics, the drag reducing action of the oscillation is related to a decreased efficiency of the momentum-pumping action of the quasi-streamwise vortices.

In order to corroborate the information one can extract from flow visualizations, we have adopted two special strategies. The first one is to remove from the calculation the pure convective
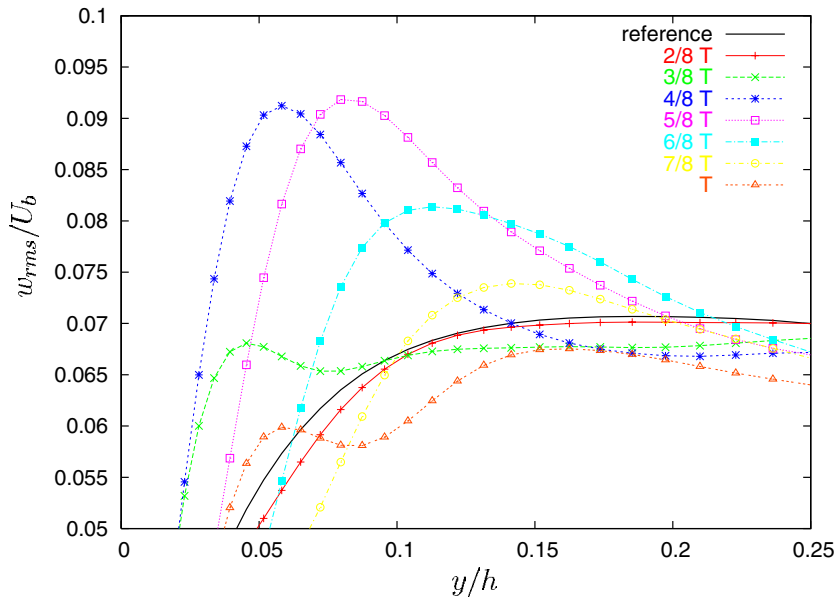
Figure 13. Evolution in time of the wall-normal distribution of w_{rms} during the first oscillation period.

motion along the streamwise direction, since in the visualizations it might overshadow the underlying dynamics. For example, in this particular flow one might be able to gain useful information from the visualization of the flow quantities in a cross-sectional y–z plane; if not removed, the streamwise convection of the structures would make the time sequence of such views useless. The removal of the convective motion has been accomplished by running the simulation in a reference frame moving at a constant speed, chosen approximately equal to the convection velocity of the turbulence structures in the near-wall region of the flow, i.e. $0.5U_b$. It is known [26] that in wall turbulence a convection velocity can be defined in a statistical sense only, and moreover that it is not constant across the vertical span of the channel. This particular value has been chosen since it allows for there to be no appreciable convection of the turbulence structures in the near-wall region, as will be clear by looking at the following 'movies', and in particular at the cross-sectional view described in figure 19. Here, it can be noted how the images in different frames smoothly follow each other in the near-wall region, while the outer part shows step changes of the velocity field between each frame.

The second adopted strategy relies on the fact that, as discussed in the preceding section, the wall motion produces a spanwise flow with a space-averaged component which is indistinguishable from the laminar analytical solution for the wall suddenly set in oscillatory motion. In the visualizations reported here, we show the fluctuations w'' of the spanwise flow, computed in the post-processing stage by subtracting the analytically calculated laminar transient flow described by equation (3). This allows a clearer appreciation of the effects of the wall motion.

We present in the following some animation frames produced from the previously described calculations. The oscillating conditions are again given by $W_m^+ = 18$ and $T^+ = 125$. The time step between successive frames is four viscous time units, and two full oscillation cycles are presented in the animations, for a total of 63 frames each.

The first frame (see figure 17) shows the top-viewed temporal evolution of the fluctuating component of streamwise velocity u, at a distance from the wall of $y^+ = 8$. The fluctuations
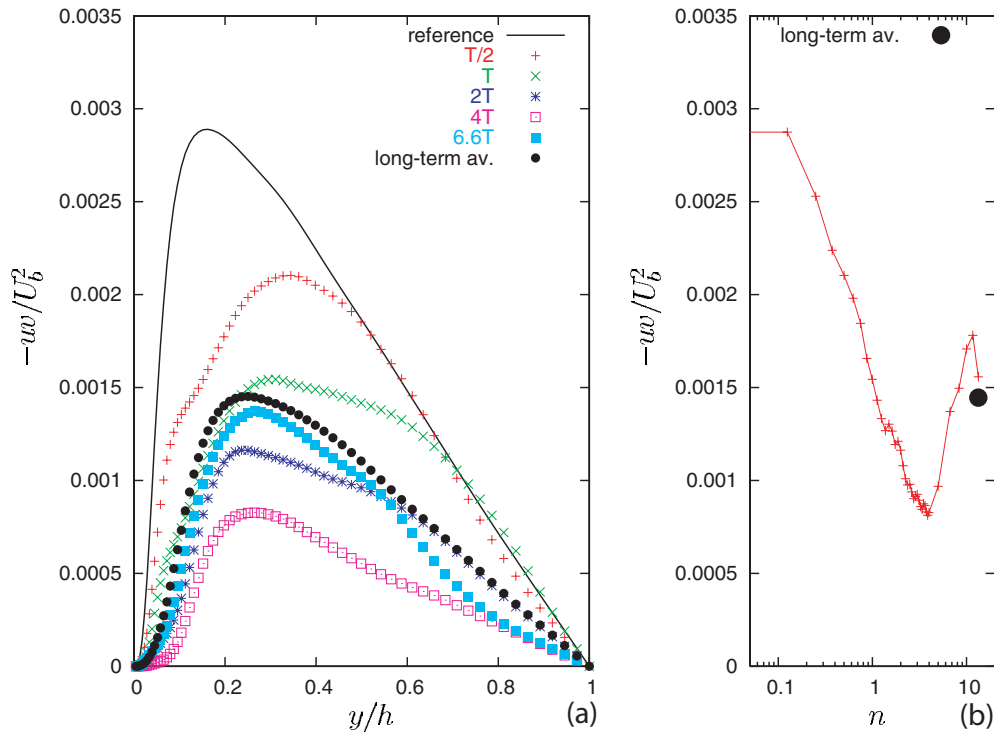
Figure 14. Evolution in time of the profiles of the Reynolds stress component $-\overline{uv}$ (a) and maximum value of $-\overline{uv}$ versus the number, n, of the oscillation cycles (b).

are computed relative to a mean velocity profile averaged in space but instantaneous in time. The flow direction goes from left to right (it can be noted how the near-wall structures are approximately fixed in the moving reference frame considered), and the red colour indicates positive values of the fluctuation. No effect of the wall motion is visible during the very first instants: at the beginning the flow is spatially organized in the well known streaky patterns, and it remains unaffected by the lateral movement of the wall until $t^+ = 16$. At $t^+ = 20$, when the wall is already moving at considerable speed, the spanwise boundary layer begins to influence the structures at this distance from the wall. As seen in figure 3, the wall shear-stress starts decreasing at $t^+ = 10$, whereas at $t^+ = 20$ it is already diminished by about 3%. Furthermore, the thickness δ_{66}^+ is ≈ 4 at $t^+ = 20$, which confirms that at this time the streaks are being merged in the region where spanwise shear stresses are significant.

As time proceeds, the effects of the wall movement are more and more evident. Low- and particularly high-speed regions orient diagonally to an angle which increases to a value of about 30° with respect to the streamwise direction, at $t^+ \approx 60$. According to the analytical solution (3), the spanwise velocity presents a time lag of $t^+ = 25$ at $y^+ = 8$ compared to the wall velocity. The maximum angle of orientation of the streaks occurs when the spanwise velocity at $y^+ = 8$ is maximum: after this instant, the streaks start to re-direct to the opposite direction. At the end of the first oscillation period, the streaks already appear significantly more homogenized and uniform. During the intermediate instants between two maximum diagonal orientations, the elongated structures orient themselves in the longitudinal direction. This happens when the spanwise velocity at this distance from the wall becomes zero.

To explain why the near-wall structures redirect angularly because of the wall movement, we recall that the upstream part of a streak lies on the wall, while the downstream part is at
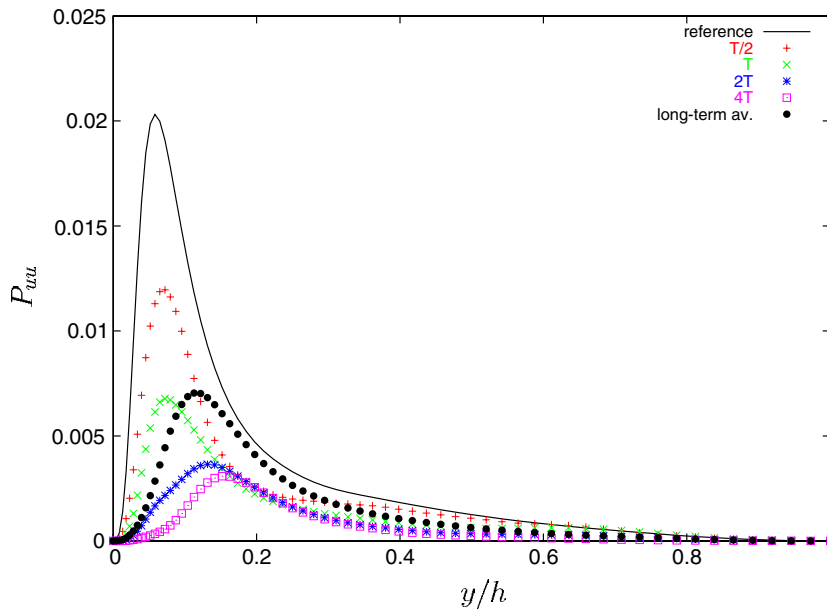
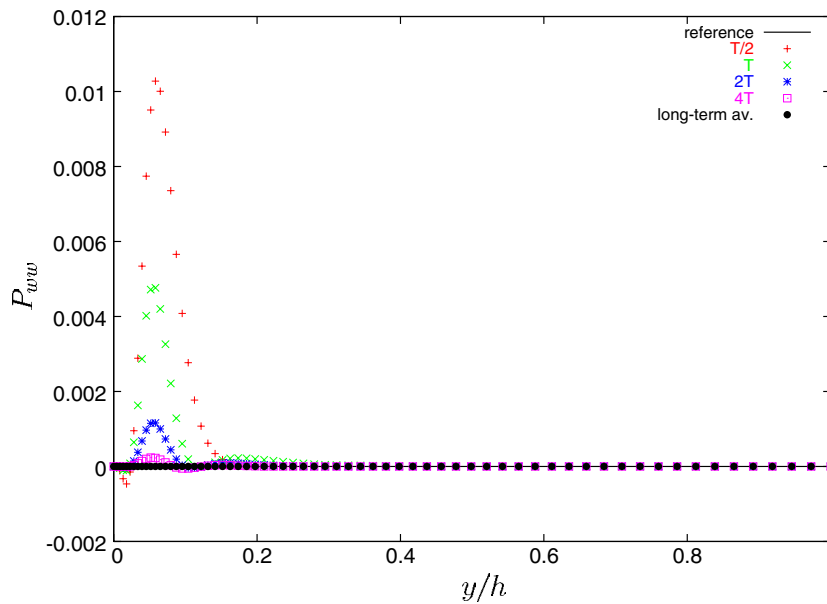**Figure 15.** Evolution in time of the TKE production term P_{uu}.

Figure 16. Evolution in time of the TKE production term P_{ww}.

a higher vertical location. When the wall motion is forced under the streaky structures, the spanwise shear stress laterally convects their upstream lower part, whereas it is less efficient on the downstream higher part. Hence, streaks show a diagonal orientation with respect to the mean flow motion. The maximum orientation occurs when the spanwise velocity induced by the Stokes layer is also at a maximum. In figure 17, we only see an horizontal section of the streaky structures, but this is sufficient to gain a feeling for their modified dynamics.

The fluctuations w'' of the spanwise velocity component are shown in figure 18, which is a top view that is analogous to the preceding one. We recall that the fluctuations w'' are computed
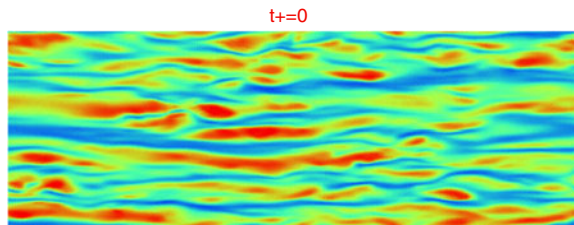
Figure 17. Top view of u velocity fluctuations at $y^+ = 8$. The streamwise direction is horizontal and the spanwise direction is vertical; the mean flow direction goes from left to right. Red indicates positive values and blue stands for negative. The structures are followed in a reference frame in uniform motion at approximately their convection velocity. The oscillating conditions are $W_m^+ = 18$ and $T^+ = 125$. The initial frame ($t^+ = 0$) corresponds to a natural turbulent flow.
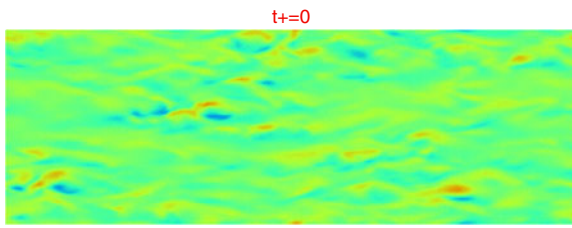

Figure 18. Top view of w'' velocity fluctuations around the laminar, analytical solution given by equation (3) at $y^+ = 8$ from the channel wall. For more information see the caption of figure 17.
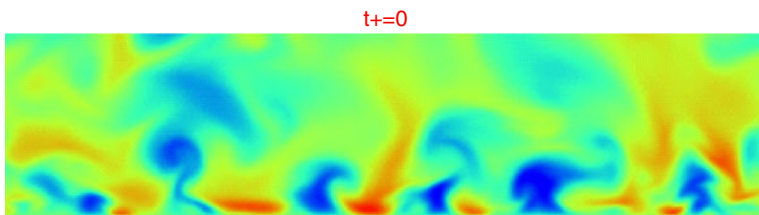

Figure 19. Cross-planar view of u velocity fluctuations. The spanwise direction is horizontal and the wall-normal direction is vertical; the wall is at the bottom and the channel centreline is at the top; the flow is into the page. For more information see the caption of figure 17.

by subtracting from the local w velocity the spatially uniform spanwise flow corresponding to the analytical solution (3). As it is well known, in the uncontrolled flow ($t^+ = 0$) there is not such clear evidence of elongated w structures. The effects of the oscillations are felt at $t^+ = 20$, similarly to the u velocity component. After this time one can observe a significant increase in the fluctuations, which is responsible for the temporary peak in the root-mean-square value of the w component, discussed in the previous section and shown in figure 12. As hypothesized in [3], the vertical momentum transfer by the quasi-streamwise vortices causes the presence of regions with $w'' > 0$, related to ejection-type events, and regions with $w'' < 0$, related to sweep-type events. This effect is particularly evident in the first half of the oscillation cycle.
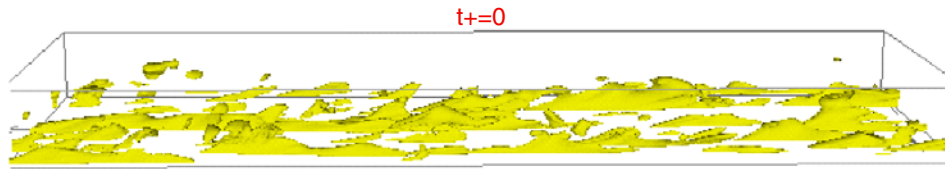
Figure 20. A three-dimensional perspective view of low-speed flow regions, indicated by isosurfaces of $u = -4u_\tau$, where for each frame the instantaneous u_τ value is considered. Flow goes from left to right.

Figure 19 shows the animation of the u velocity fluctuations in a cross-sectional y–z plane. For such visualizations the choice of a reference frame in motion with a speed similar to the convection velocity of the turbulence structures has proven to be essential for obtaining a vivid picture of sections of the low-speed streaks as they evolve with time. At the beginning the characteristic cross-sectional shape of low- and high-velocity regions alternating in the spanwise direction can be clearly recognized. In this view the effect of the moving wall becomes apparent a little earlier, since the very near-wall region is visible. It basically determines a lateral shift in the lower part of the structures, with a vertical stacking of high-speed regions below low-speed pockets, as hypothesized by Quadrio and Sibilla [3]. This stacking is particularly evident in the first half of the oscillation cycle. After one entire cycle of oscillation the spatial organization of the streaks is significantly modified and their intensity reduced, but, more importantly, the near-wall region no longer presents significant fluctuations. The alternate pattern of high- and low-speed regions, with the high-speed regions intruding beneath the low-speed fluid, can still be observed at later times, but to a much lesser extent.

Flow visualizations of a transient flow like the present one could be affected by a transient change in the scaling parameter. If, for example, the longitudinal velocity fluctuations are scaled with the friction velocity, one might expect a significant effect on the observed pictures when the actual reduction of u_τ with time is taken into account. The friction velocity actually decreases more than 20% from its initial value during the time interval considered for the animated frames, as it can be estimated from figure 6. To verify that this change in the threshold level causes no qualitative effect, figure 20 reports a three-dimensional view of the low-speed flow regions as time evolves, shown as isosurfaces at the level $u = -4u_\tau$. This time the threshold, i.e. the friction velocity, is not kept fixed at the value of the reference flow, but it is set according to its instantaneous value. One can easily recognize from the analysis of the animation that after one oscillation period the flow patterns are significantly modified, notwithstanding the time-decreasing threshold level. At $t^+ = 0$, elongated portions of fluid with low streamwise velocity are evident, which start being disrupted at the very beginning of the wall motion. The moving reference frame allows a clear appreciation of the link between the low-speed regions and the vertical motion which leads them away from the wall (ejections). A relatively small convection of the low-speed pockets can be observed in the outer flow, where it is known [26] that the convection velocity of turbulent fluctuations increases, and hence becomes superior to the adopted speed of the moving reference frame. As time proceeds, the appearance of elongated streaks of the low-speed fluid is remarkably reduced.

These flow visualizations give sharp visual support to the idea that the oscillation of the wall significantly alters the turbulence cycle. Du et al [29] recently observed how some turbulent drag reduction techniques, like, for example, the application of transverse travelling waves in the near-wall region, efficiently yield to a drag reduction effect and produce a near-wall flow structure which is significantly altered when compared to the uncontrolled flow. However, they also surmise

that other techniques, including the spanwise wall oscillation, achieve a similar amount of drag reduction while apparently maintaining the same qualitative near-wall flow structure. From the flow visualizations presented in this paper one can, however, obtain the impression that the flow over the oscillating wall is qualitatively different from the natural turbulent flow.

6. Conclusions

The initial transient of a turbulent channel flow suddenly subjected to harmonic oscillations of the walls has been studied by means of DNSs of the Navier–Stokes equations.

It is found that the spanwise flow at the very beginning of the wall motion is composed by the turbulent flow superimposed on a laminar flow which is coincident with the analytical solution of the boundary layer equations for the case of a wall suddenly set in oscillatory motion.

The timescales on which the spanwise and the longitudinal flows adapt to the new condition and reach a new equilibrium state are well separated; the former is shorter and only depends on the period of the wall oscillation, while the latter varies both with the period of the oscillation and, more importantly, with the maximum wall velocity.

The increase in the duration of the transient period for increasing maximum wall velocities is particularly relevant, since it implies that in laboratory experiments the position of the measuring probe after the leading edge of the oscillating wall must be chosen with care, on the basis of the highest maximum wall velocity considered in the experiments. It appears that some experimental drag reduction measurements over an oscillating wall available in the literature might have been conducted in a position where the flow had not fully adapted to the new equilibrium condition, at least for some values of the oscillating wall parameters.

The turbulent flow is shown to adapt to its long-term state through a non-monotonic process, where the reduction of the longitudinal friction leads initially to a local minimum and then to a partial recovery towards the long-term value. Similar behaviour is presented by the distribution of the root-mean-square values of the velocity fluctuations.

Flow visualizations of the early moments of motion allow for the observation of the interaction amongst the moving wall and an overriding turbulent flow field which was previously undisturbed, thus enhancing the capability of understanding how the alternate motion of the wall is able to alter the self-sustaining turbulence cycle near the wall.

References

[1] Jung W J, Mangiavacchi N and Akhavan R 1992 Suppression of turbulence in wall-bounded flows by high-frequency spanwise oscillations *Phys. Fluids* A **4** 1605–7
[2] Baron A and Quadrio M 1996 Turbulent drag reduction by spanwise wall oscillations *Appl. Sci. Res.* **55** 311–26
[3] Quadrio M and Sibilla S 2000 Numerical simulation of turbulent flow in a pipe oscillating around its axis *J. Fluid Mech.* **424** 217–41
[4] Laadhari F, Skandaji L, and Morel R 1994 Turbulence reduction in a boundary layer by a local spanwise oscillating surface *Phys. Fluids* **6** 3218–20
[5] Choi K-S 2002 Near-wall structure of turbulent boundary layer with spanwise-wall oscillation *Phys. Fluids* **14** 2530–42
[6] Di Cicca G M, Iuso G, Spazzini P G and Onorato M 2002 PIV investigation of turbulent boundary layer manipulated by spanwise wall oscillations *J. Fluid Mech.* **467** 41–56
[7] He S and Jackson J D 2000 A study of turbulence under conditions of transient flow in a pipe *J. Fluid Mech.* **408** 1–38
[8] Kannepalli C and Piomelli U 2000 Large-eddy simulation of a three-dimensional shear-driven turbulent boundary layer *J. Fluid Mech.* **423** 175–203
[9] Jiménez J, Uhlmann M, Pinelli A and Kawahara G 2001 Turbulent shear flow over active and passive porous surfaces *J. Fluid Mech.* **442** 89–117

[10] Chung Y M and Luo K H 2002 DNS of a turbulent flow with sudden change in pressure gradient *Proc. 9th European Turbulence Conf.; Advances in Turbulence* vol 9, ed I P Castro, P E Hancock and T G Thomas p 842

[11] Moin P, Shih T H, Driver H and Mansour N 2000 Direct numerical simulation of a three-dimensional turbulent boundary layer *Phys. Fluids* A **2** 1846–53

[12] Sendstad O and Moin P 1991 On the mechanics of 3-D turbulent boundary layers *8th Symp. on Turbulent Shear Flows (Technical University of Munich)* vol 1, p 5-4-1

[13] Coleman G N, Kim J and Le A T 1996 A numerical study of three-dimensional wall-bounded flows *Int. J. Heat Fluid Flow* **17** 333–42

[14] Le A T, Coleman G N and Kim J 2000 Near-wall turbulence structures in three-dimensional boundary layers *Int. J. Heat Fluid Flow* **21** 480–8

[15] Orlandi P and Fatica M 1997 Direct simulations of turbulent flow in a pipe rotating about its axis *J. Fluid Mech.* **343** 43–72

[16] Spalart P 1989 Theoretical and numerical study of a three-dimensional turbulent boundary layer *J. Fluid Mech.* **205** 319–40

[17] Dhanak M R and Si C 1999 On reduction of turbulent wall friction through spanwise oscillations *J. Fluid Mech.* **383** 175–95

[18] Choi K-S, DeBisschop J R and Clayton B R 1998 Turbulent boundary-layer control by means of spanwise-wall oscillation *AIAA J.* **36** 1157–62

[19] Quadrio M and Luchini P 2001 A 4th order accurate, parallel numerical method for the direct simulation of turbulence in Cartesian and cylindrical geometries *Proc. 15th AIMETA Conf. on Theoretical and Applied Mechanics*

[20] Kim J, Moin P and Moser R 1987 Turbulence statistics in fully developed channel flow at low Reynolds number *J. Fluid Mech.* **177** 133–66

[21] Moser R, Kim J and Mansour N N 1999 Direct numerical simulation of turbulent channel flow up to $Re_\theta = 590$ *Phys. Fluids* **11** 943–5

[22] Jeong J, Hussain F, Schoppa W and Kim J 1997 Coherent structures near the wall in a turbulent channel flow *J. Fluid Mech.* **332** 185–214

[23] Choi K-S and Clayton B R 2001 The mechanism of turbulent drag reduction with wall oscillation *Int. J. Heat Fluid Flow* **22** 1–9

[24] Panton R 1995 *Incompressible Flow* 2nd edn (New York: Wiley–Interscience)

[25] Choi J-I, Xu C-X and Sung H J 2002 Drag reduction by spanwise wall oscillation in wall-bounded turbulent flows *AIAA J.* **40** 842–50

[26] Kim J and Hussain F 1993 Propagation velocity of perturbations in turbulent channel flow *Phys. Fluids* A **5** 695–706

[27] Skandaji L 1997 Etude de la structure d'une couche limite turbulente soumise à des oscillations trasversales de la paroi *PhD Thesis* Ecole Centrale de Lyon

[28] Trujillo S M, Bogard D G, and Ball K S 1997 Turbulent boundary layer drag reduction using an oscillating wall *28th AIAA Fluid Dynamics Conf.; 4th AIAA Shear Flow Control Conf.*

[29] Du Y, Symeonidis V, and Karniadakis G E 2002 Drag reduction in wall-bounded turbulence via a transverse travelling wave *J. Fluid Mech.* **457** 1–34